

### 3. Storage Ring

The CANDLE synchrotron light source general design is based on a 3 GeV electron energy storage ring, full energy booster synchrotron and 100 MeV S-Band injector linac. The storage ring of the accelerator complex is the major facility that provides high brilliance X-ray beams from the bends and insertion devices. The ring has a circumference of 216m that is divided into 16 Double-Bend Achromatic (DBA) sections with a single cell length of 13.5 m. Each cell contains a 4.8 m long straight section for installation of insertion devices, injection system and radio frequency cavities.

The full energy booster synchrotron operating with a repetition rate of 2 Hz and nominal pulse current of 10 mA provides the storage of 350 mA current in less than 1 min. The storage ring circumference of 216m gives the harmonic number  $h=360$  (number of RF periods per ring) for the accelerating mode wavelength 60 cm (499.654 MHz frequency) that results in a convenient decomposition of  $(360=2^3 \cdot 2^2 \cdot 5)$  thereby allowing the possibility of ring operation with many different bunch patterns.

The design of the machine is based on conventional technology operating at normal conducting temperature. However, if the demand of the user community requires the extension of the photon spectral range to hard X-ray region, superconducting wigglers may be installed. Table 3.1 presents the main parameters of the storage ring.

**Table 3.1 Main parameters of CANDLE storage ring.**

Parameter	Value
Energy E (GeV)	3
Circumference (m)	216
Current I (mA)	350
RF frequency (MHz)	499.654
Harmonic number	360
Number of lattice periods	16
Straight section length (m)	4.8
Lattice type	DBA
Bending radius $\rho$ (m)	7.385

Optimization of the storage ring performance has been made based on the following criteria:

- Photon beams from the bending magnets and the insertion devices need to cover the energy range of 0.1-50 keV with high spectral flux and brightness.
- The storage ring should have sufficient dynamical aperture and has to provide for stable and reproducible operation of the facility with a long beam lifetime;
- For time dependent processes such as injection and storage, flexible operation and control are required to minimize beam losses and to provide reproducible electron beam positioning during filling.
- The ability to accommodate many different bunch patterns (single and multi-bunch operation) for time resolved experiments, needs to be incorporated into the design.

To meet these challenges and to approach the high level of machine performance achieved in other numerous light sources which use standard conventional technology, a detailed study of the main physical processes in the storage ring has been performed.

### 3.1 Magnetic Lattice

The optics of magnetic structure of the storage ring is the basic part of the machine that defines the main parameters of the stored electron beam. The number of magnetic lattice periods has been determined based on the balance of having high efficiency usage of the straight sections for insertion devices (~75%), the comparatively low beam emittance (below 10 nm-rad), about 5 m longer length of straight section in each cell and the facility to be cost effective. Taking into account that injection devices will occupy one straight section, and three straight sections are intended for RF cavities, the number of cells has been determined to be 16. With 216 m ring circumference and DBA lattice structure of the single cell, each straight section has the length of 4.8m. The free space of 4 m length is then available for the wiggler or undulator insertion devices.

#### 3.1.1 Figure of Merits and Lattice Design

The basic consideration that underlies the magnetic structure (lattice) design for synchrotron light sources is the achievement of high brilliance of the photon beams thus to realize the full potential from insertion devices. The high brightness of the photon beams is achieved by having a high brightness of the electron beam. In addition to the optimization of the radiation characteristics of the photon source, the design should be accompanied by the corresponding study of the dynamical aperture of the machine to obtain a good stable electron beam with reproducible beam positioning during the stored time.

**Emittance.** The emittance of a particle beam in an electron storage ring is determined by equilibrium between the quantum excitation, which causes a transverse kick for individual particles, and the radiation damping of the betatron oscillations. The resulting horizontal equilibrium emittance is given by the expression [1]

$$\varepsilon_x = \frac{C_q \gamma^2 H_{mag}}{J_x \rho} \quad (3.1.1)$$

where  $C_q = 3.84 \cdot 10^{-13} m$ ,  $\gamma$  is the particle Lorentz factor,  $\rho$  is the bending radius,  $J_x$  is the horizontal damping partition number and  $H_{mag}$  is the dispersion invariant.

In a perfect machine there is no dispersion in the vertical plane so that vertical emittance is zero. However, in a real machine, the magnet imperfections and misalignments cause a coupling between the horizontal and vertical planes. The CANDLE design specification is aimed to keep this coupling at the level of less than 1 %, so that  $\varepsilon_y \approx 0.01\varepsilon_x$ .

The choice of one of the driving parameters of the machine – the particle bending radius ( $\rho = 7.385m$ ) - is made by aiming to have a photon critical energy of about 8 keV from dipole sources for 3 GeV electrons energy and a nominal magnetic field in the dipoles of  $B = 1.345 T$ . This value of magnetic field permits a good quality field with tolerance of  $\Delta B / B < 10^{-4}$  in the magnet aperture using conventional technology for dipole production.

In a separated functions machine (i.e. zero field gradient in the dipoles), the damping partition number is approximately equal to 1. The quantity  $J_x$  can be increased by a factor of about half as much again (factor of 1.5 decrease in emittance) by introducing vertical focusing in the dipole magnets. In CANDLE, this is achieved by using a SPEAR3 [2] type dipole magnet design with a magnetic field index of  $n=18$ .

The next important parameter to achieve low emittance for the electron beam is the minimization of the dispersion invariant  $H_{mag}$  by a proper choice of the lattice structure and the tunes of the betatron oscillations. The CANDLE lattice design is based on the extended double bend achromatic lattice as the most compact structure used in low emittance storage rings. Numerous studies of the linear and non-linear optics of the machine lead us to a design that uses two dipole magnets interspaced with focusing central quadrupole and two focusing-defocusing quadrupole doublets upstream and downstream of the bending sections, thereby providing more flexibility in the adjustment of transverse dimensions. This arrangement of the focusing lattice allowed us to have 16 periods over the ring with 4.8m long straight section in each cell for installation of wigglers, undulators, RF cavities and injection devices.

Another factor of two in emittance reduction is achieved by using low dispersion in the straight sections at the level of 0.18m. Taking into account the necessity for chromaticity corrections, the betatron tune values have been optimized to  $Q_x=13.22$  in horizontal and  $Q_y=4.26$  in vertical planes respectively.

**Brightness.** For a Gaussian beam distribution, the brightness is given by

$$B \left[ \frac{\text{photons}}{\text{sec} \cdot \text{mm}^2 \cdot \text{mrad}^2 \cdot 01\% \text{BP}} \right] = \frac{N_{ph}}{4\pi^2 \sigma_{px} \sigma_{px'} \sigma_{py} \sigma_{py'}} \quad (3.1.2)$$

where  $N_{ph}$  is the photon flux,  $\sigma_{pu}, \sigma_{pu'}$  are the effective rms size and divergence of the photon source in the horizontal ( $u = x$ ) and vertical ( $u = y$ ) planes. High brightness is required for experiments that involve samples or optics with very small phase space acceptance or techniques that exploit beam coherence and is an important figure of merit of synchrotron radiation sources. The photon beam size  $\sigma_{pu}$  and divergence  $\sigma_{pu'}$  are the result of folding diffraction with electron beam size and divergence, and at the source point of zero dispersion lattice is given by [3]

$$\sigma_{pu} \sigma_{pu'} = \sqrt{(\epsilon_u \beta_u + \sigma_r^2)(\epsilon_u \gamma_u + \sigma_{r'}^2)} \quad (3.1.3)$$

where  $\gamma_u = (1 + \alpha_u^2) / \beta_u$ ,  $\alpha_u = -\beta'_u / 2$ ,  $\beta_u$  is the usual betatron function at the source point,  $\sigma_r, \sigma_{r'}$  are the diffraction limited rms radial photon beam size and divergence that depend on both the photon wavelength of interest  $\lambda$  and the length of the source  $L$  (undulator or wiggler length) as  $\sigma_r^2 = \lambda L / 8\pi^2$  and  $\sigma_{r'}^2 = \lambda / 2L$ . As usual, in further considerations it is assumed that in the middle of the insertion devices  $\alpha_u = 0$ .

The maximum level of brightness is reached only at the so-called diffraction limit when the beam emittance is about equal to a fraction of the wavelength of the radiation. As an

example, a diffracted limited beam capable of producing 10 keV X-rays would have an emittance of 0.01 nm-rad. The optimum value of the betatron function at the source point for the diffraction limited case is then  $\beta^* = \sigma_r / \sigma_{r'} = L/2\pi$  and depends only on the length of the undulator or wiggler.

The new 3<sup>rd</sup> generation intermediate energy storage rings under design or construction have design values of horizontal emittance 3-15 nm-rad [4]. Therefore, the dependence of the spectral brightness on the betatron value at the source point is largely visible only in the IR and UV regions of the excited photons [5]. Fig.3.1.1 presents the spectral brightness for the ID source as a function of radiated photon energy for various horizontal betatron functions at the source point. The electron beam emittance is taken equal to 8.4 nm-rad, dispersion at the source point is zero and the length of ID is 4m. The quantity on the vertical axis is the inverse transverse phase area  $S = 2\pi\sigma_{px}\sigma_{px'}$  of the photon beam in  $mm^{-1} \cdot mrad^{-1}$ . It is evident, that decreasing the betatron function at the source point by one order of magnitude (from 10m to 1 m) gives a gain in spectral brightness of less than 10% in soft X-ray region (photon energy range 0.5-2 keV), less than 3% in X-ray region 2-8 keV and it is actually independent on low beta lattice at photon energies higher than 8 keV.

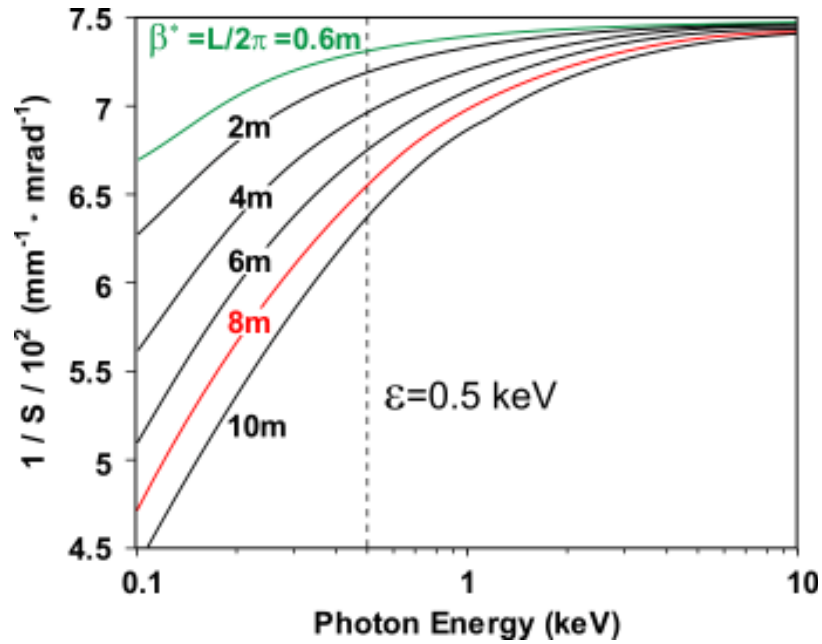


**Fig.3.1.1 The spectral brightness behavior for various betatron functions at the source point. Achromatic lattice ( $\eta = 0$ ), an electron beam emittance  $\epsilon_x = 8.4nm \cdot rad$ .**

For a real electron beam that excites the synchrotron radiation as its travel along the ID, the photon beam is diluted due to electron beam oscillating trajectory and the electron beam transverse size variation. Geometrical considerations increase apparent source size from the ideal source size in the middle of the ID given by (3.1.3). A diluted photon beam emittance  $\epsilon_{ph}$  along the optical axis of the ID is then given by [6]

$$\epsilon_{ph}^2 = \sigma_{pu}^2 \sigma_{pu'}^2 = \epsilon_u^2 \left(1 + L^2/12\beta_u^2\right) + \epsilon_u \sigma_{r'}^2 \beta_u + \epsilon_u \sigma_{r'}^2 p_u / \beta_u + d_u^2 \sigma_{r'}^2 \quad (3.1.4)$$

with

$$p_u = L^2/12 + d_u^2/\sigma_r^2, \quad d_x^2 = \sigma_\epsilon^2 \eta_x^2 + \sigma_r^2 + a^2, \quad d_y^2 = \sigma_r^2.$$

Here  $a = \lambda_p K / (2\pi\gamma)$  is the electron beam oscillations amplitude that causes the widening of the source size,  $\lambda_p$  is the undulator period,  $K$  is the ID strength parameter,  $\sigma_\epsilon$  is the rms energy spread in electron beam,  $\eta_x$  is the horizontal dispersion function. The betatron and dispersion functions divergences are assumed to be zero ( $\alpha = 0, \eta'_x = 0$ ), that is the usual case for the DBA non-zero dispersion lattice design.

For the arbitrary electron beam emittance the optimal  $\beta_u^*$  in the middle of ID for the fixed photon energy is then given by algebraic cubic equation [7]

$$\beta_u^{*3} - p_u \beta_u^* - q_u = 0, \quad (3.1.5)$$

with  $q_u = L^3 \epsilon_u / 3\lambda$ . The single real positive solution of the equation is given by [6]

$$\beta_u^* = \sqrt{p_u/3} \begin{cases} 2 \cos(1/3 \cdot \arccos \mu), & \mu < 1 \\ \left[ (\mu + \tilde{\mu})^{1/3} + (\mu - \tilde{\mu})^{1/3} \right], & \mu > 1 \end{cases} \quad (3.1.6)$$

with  $\mu = q_u / 2\sqrt{(p_u/3)^3}$  and  $\tilde{\mu} = \sqrt{\mu^2 - 1}$ . Actually, the optimum beta function  $\beta^*$  for the given photon wavelength defines the optimum electron beam size and divergence in the middle of ID that give the maximum spectral brightness. Fig.3.1.2 shows the dependence of CANDLE spectral brightness from the emitted photon energy for various horizontal beta values in the middle of ID. The CANDLE achromatic lattice ( $\eta = 0$ ) with the horizontal emittance of 18 nm-rad and the dispersive lattice ( $\eta = 0.18m$ ) with the horizontal emittance of 8.4 nm-rad are shown for comparison. Dashed line gives the brightness for optimal beta values (3.1.6) associated with each photon energy for the dispersive lattice.

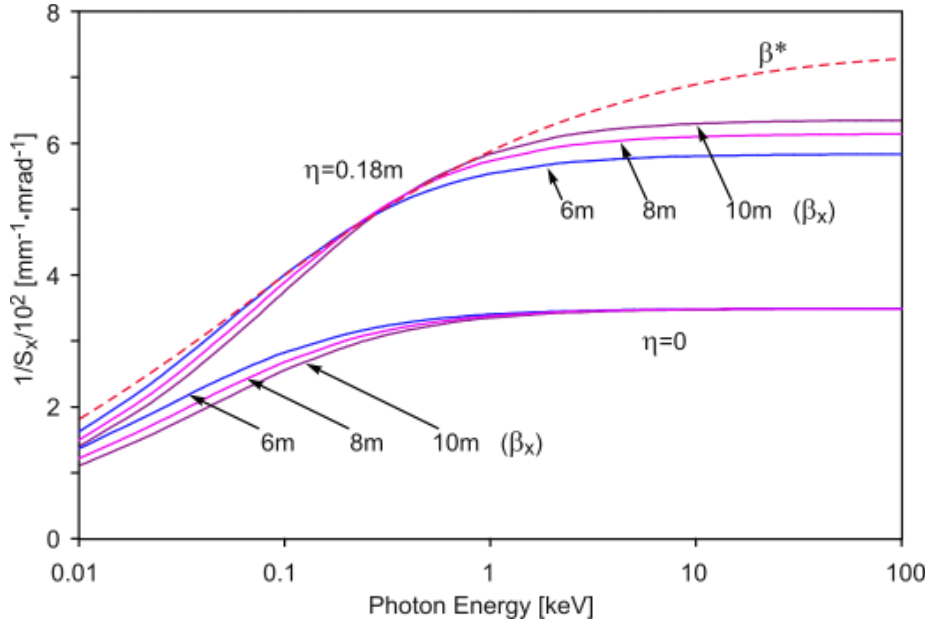


**Fig. 3.1.2 The spectral brightness versus photon energy for various horizontal beta. Shown are: CANDLE achromatic lattice ( $\eta = 0$ ), dispersive lattice ( $\eta = 0.18m$ ) and optimal beta for dispersive lattice (dashed line).**

For the dispersive lattice the improvement of the brightness with small beta is essential only for the photon energies below 0.1 keV. Starting from 0.5 keV the brightness increases with larger betatron function, and in the energy range of higher than 5 keV, the brightness actually does not depend on the photon energy. An important feature is that for dispersive lattice, which reduces the horizontal emittance to 8.4 nm-rad, the brightness is about twice larger than the brightness obtained with the achromat lattice that gives an electron beam emittance of about 18 nm-rad. Recognizing the significant improvements in the dynamical aperture of the ring and the more effective beam injection performance with a large horizontal beta value, the CANDLE lattice has been optimized to a horizontal beta value of 7.9m in the middle of ID (long straight section).

In the vertical plane, in addition to high brightness approach, a low vertical betatron function is required in the straight section to reduce the linear and non-linear focusing effects of the wiggler [8]. Fig. 3.1.3 shows the spectral brightness for various vertical beta functions for CANDLE dispersive lattice and 1% coupling. The vertical emittance is 0.084 nm-rad.

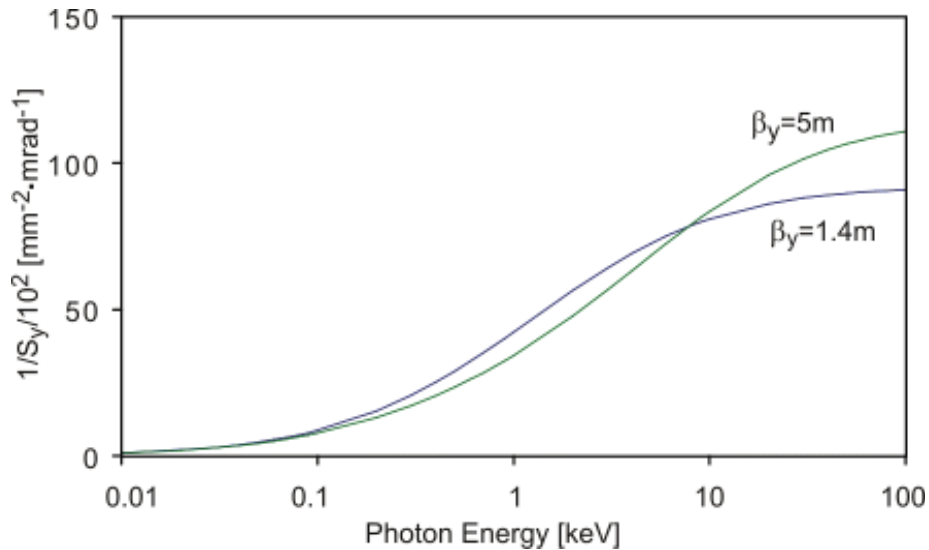


**Fig. 3.1.3 Spectral brightness for various vertical betatron functions.**

The simulation of wiggler related effects for CANDLE has been performed based on the assumption that the wiggler poles are sufficiently long in the horizontal direction, so that there are only longitudinal and vertical field components not affecting the vertical motion of the particles. Taking into account the above-discussed features of photon and electron beams performance and the requirement to have a sufficient vertical dynamical aperture of the ring, the vertical betatron function in the middle of the straight section is optimized to  $\beta_y = 4.85m$ .

### 3.1.2 Standard Cell and Linear Optics

The standard cell of the storage ring is based on the Double – Bend Achromatic (DBA) system that consists of two gradient dipole magnets (B) with central focusing quadrupole (QFC) and two quadrupole doublets (QF, QD) upstream and downstream of the bending section (Fig. 3.1.4). The total length of the standard cell of 13.5m allows having 16 periods of identical DBA lattices along the ring with 216 m in circumference. The standard cell contains two families of focusing and defocusing sextupoles (SF, SD) for the linear chromaticity correction.

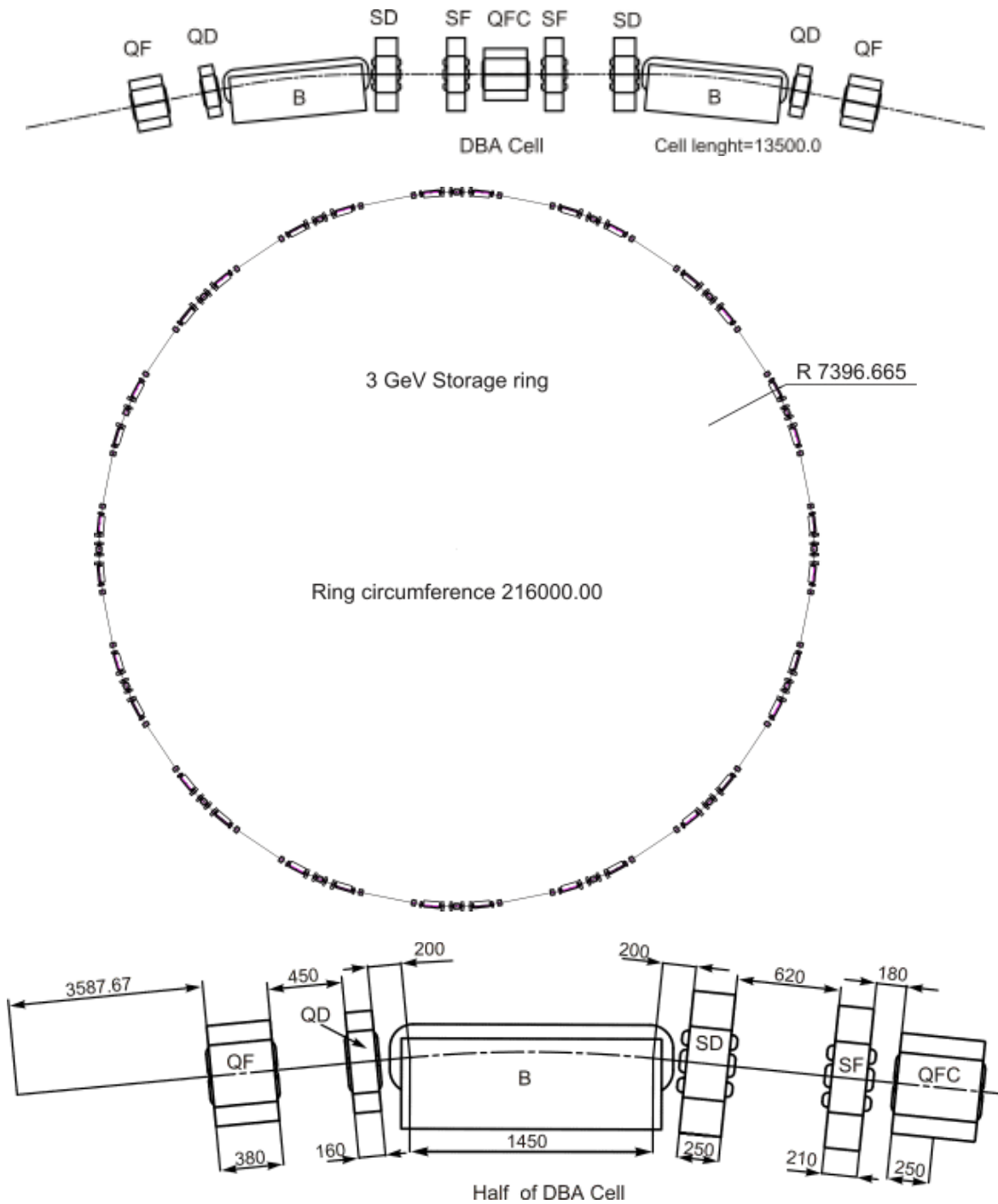


**Fig. 3.1.4 Standard DBA Cell and Ring Arrangement.**

The geometry of the standard cell is adapted to have necessary space for Beam Position Monitors, vacuum chamber valves, pumping stations and includes having a 4.8 m long straight section in each cell that is available for insertion devices, RF system and injection system. In total, 12 straight sections will be available for insertion devices.

The standard cell geometry has been optimized based on the requirement of obtaining the minimum sextupole field for chromaticity compensation thus improving the dynamical aperture of the machine. The optimization has been performed to meet the given values of the betatron tunes and beta functions in the middle of the straight section discussed in the previous section.

The working point of the horizontal and vertical betatron oscillations are  $Q_x = 13.22$  and  $Q_y = 4.26$  which is far enough from the nearest resonances in the resonance diagram of the storage ring (Fig. 3.1.5). Figure 3.1.6 presents the optical functions for one standard cell.

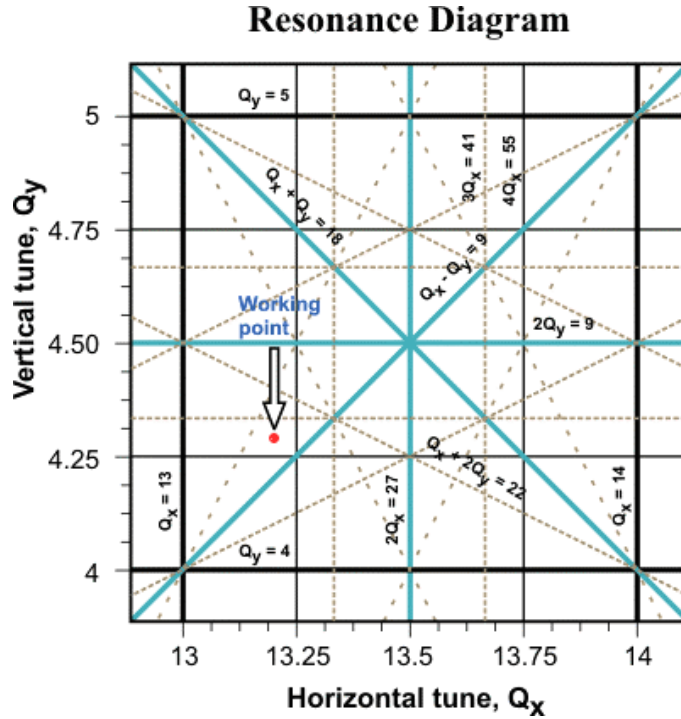


**Fig. 3.1.5** Resonance diagram and working point of betatron tunes.

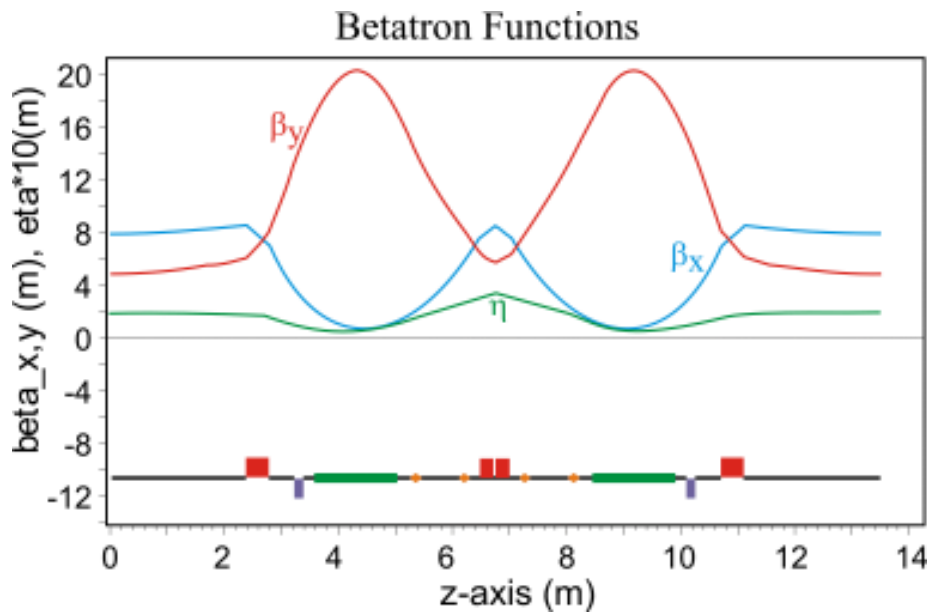


**Fig. 3.1.6** Betatron  $\beta$  and dispersion  $\eta$  functions in one standard DBA cell.

The dispersion at the straight section of the lattice is at the level of 0.18m that with the given cell arrangement provides the horizontal beam emittance 8.4 nm-rad. The lattice optics can be easily tuned to achromatic lattice by adjusting the strength of the central quadrupole QFC. The natural horizontal emittance of the beam then approaches 18 nm-rad. This option for the lattice is very convenient for the initial stage of the facility operation, during the storage ring commissioning.

The lattice design and the quadrupole gradient budget allow the facility operation at high horizontal betatron tune  $Q_x = 14.22$  thus reducing the horizontal beam emittance to 5.6 nmrad in the expenses of the dynamical aperture reduction. This option will be studied after the commissioning of the storage with the nominal values of tunes shown on the resonance diagram. Table 3.1.1 presents the main parameters of the standard cell and the linear optics of the storage ring.

**Table 3.1.1 Parameters of standard cell and linear optics.**

Parameter	Value
Quadrupole strength QF, QD, QFC ( $m^{-2}$ )	1.65 / -1.29 / 1.7
Dipole field (T)	1.354
Dipole gradient strength ( $m^{-2}$ )	0.33
Horizontal tune $Q_x$	13.22
Vertical tune $Q_y$	4.26
Horizontal $\beta$ in the straight (m)	7.89
Vertical $\beta$ in the straight (m)	4.87
Dispersion $\eta$ in the straight (m)	0.18
Peak horizontal beta $\beta_{xmax}$ (m)	8.62
Peak vertical beta $\beta_{ymax}$ (m)	17.08
Momentum compaction $\alpha$	0.002
Horizontal chromaticity $\xi_x$	-18.914
Vertical chromaticity $\xi_y$	-14.86

### 3.1.3 Electron Beam Parameters

The electron beam parameters of the machine follow from the main specifications of the photon beams characteristics, stable machine operating conditions and the adopted optics for the regular lattice. With dispersion  $\eta = 0.18m$  in the middle of the straight section, the design provides the equilibrium emittance of  $\epsilon_x = 8.4nm$  in the horizontal plane. In the vertical plane, the coupling-correction system is expected to achieve 1% coupling. The resulting vertical emittance will be then on the order of  $84 pm \cdot rad$ .

**Table 3.1.2 Electron beam parameters**

Parameter	Value
Energy (GeV)	3
Coupling (%)	1
Energy loss per turn (MeV)	0.97
Horizontal emittance (nm)	8.4
Vertical emittance (nm)	0.084
Relative energy spread (%)	0.104
Damping times (ms)	
Horizontal $\tau_x$	3.822
Vertical $\tau_y$	4.484
Longitudinal $\tau_z$	2.455

The rms sizes and divergences of the electron beam at the source point, i.e. in the middle of the dipole magnet and in the center of the long straight section, are given in Table 3.1.3

**Table 3.1.3 Electron beam sizes at the source point.**

Parameter	Dipole	Insertion
$\sigma_x$ ( $\mu m$ )	128	314
$\sigma_{x'}$ ( $\mu rad$ )	92	32.6
$\sigma_y$ ( $\mu m$ )	41	20
$\sigma_{y'}$ ( $\mu rad$ )	2.05	4.16

The rms horizontal beam size  $\sigma_x$  and the divergence  $\sigma_{x'}$  include the contribution from the non-zero dispersion  $\eta$  and are given by

$$\sigma_x^2 = \epsilon_x \beta_x + \sigma_\epsilon^2 \eta^2, \quad \sigma_{x'}^2 = \epsilon_x \frac{1 + \alpha_x^2}{\beta_x} + \sigma_\epsilon^2 \eta'^2 \quad (3.1.7)$$

with  $\alpha = -\beta'/2$  and  $\sigma_\epsilon$  rms particle relative energy spread.

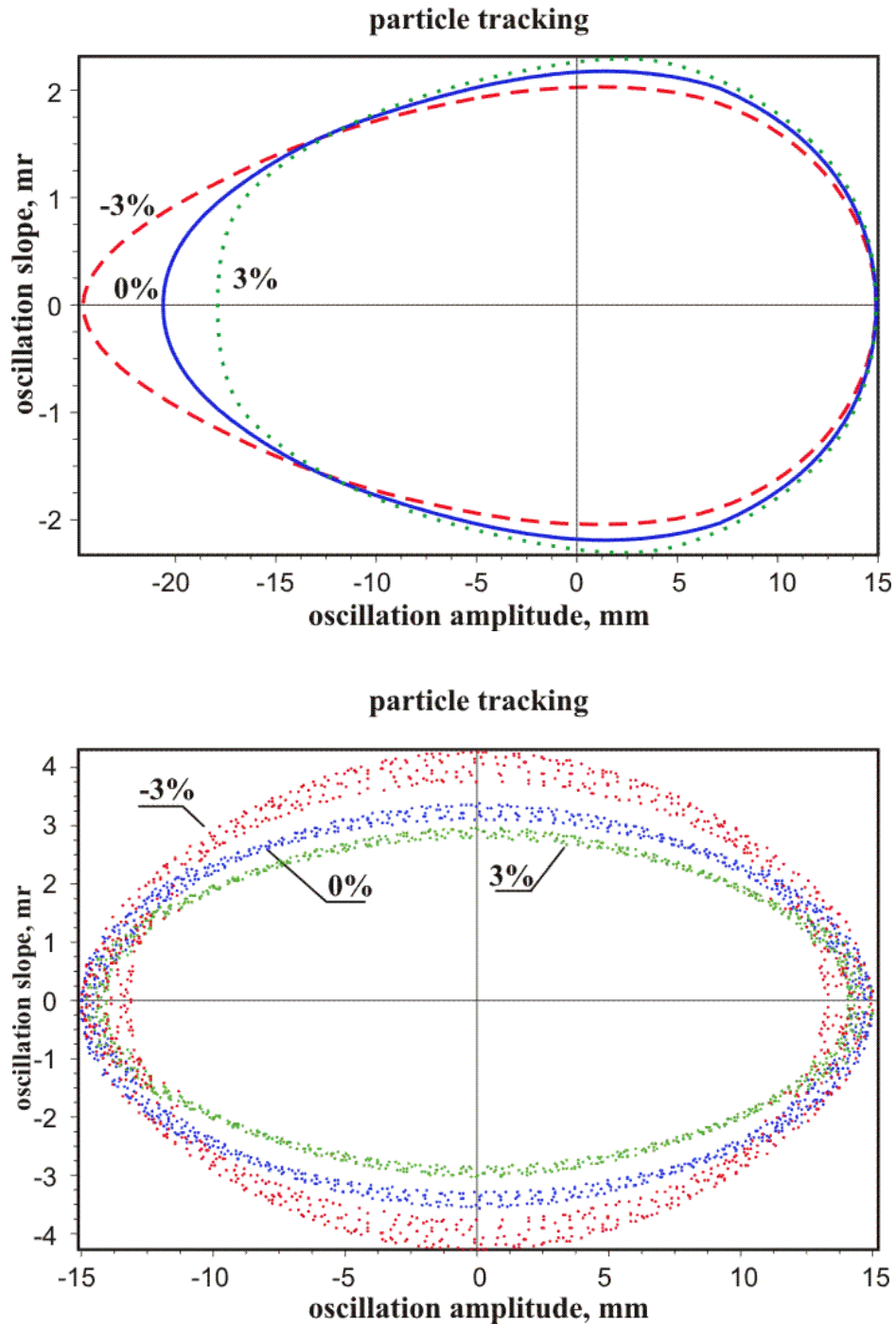
### 3.1.4 Chromaticity Compensation and Dynamical Aperture

An off-energy particle in the linearly focusing lattice of the storage ring experiences additional extra focusing (defocusing) in the quadrupoles within the lattice that results in a tune shifts of the off-energy particles. This quantity known as the natural chromaticity of the ring is given by:

$$\xi_{x,y} = \frac{\Delta Q_{x,y} / Q_{x,y}}{\Delta E / E} = -\frac{1}{4\pi} \oint K(s') \beta_{x,y}(s') ds' \quad (3.1.8)$$

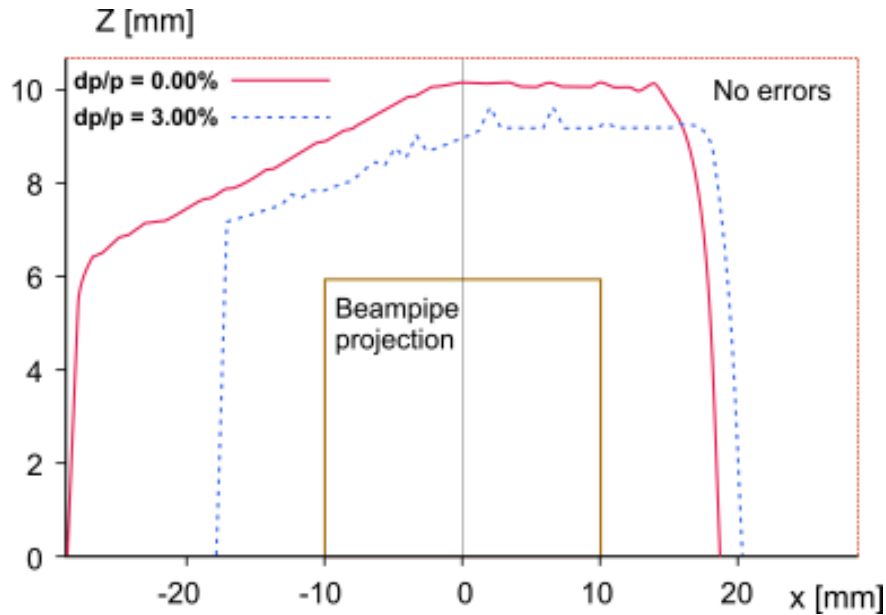
where  $K$  is the quadrupole strength. The natural chromaticity is negative in a linear focusing lattice of the machine since the high energy particles experience less focusing with respect to design particle while passing through the quadrupole magnet. The negative chromaticity of the machine is the source of so-called ‘‘head-tail’’ instability [9,10] and  $\xi_{x,y}$  must be adjusted to be zero or slightly positive from its naturally occurring negative values. This is normally achieved with sextupole magnets placed in the regions of the lattice where the dispersion is finite. Additional optimization is necessary to adjust the sextupole location to minimize the number of the sextupoles and to reduce the sextupole field that is necessary to compensate the chromaticity. An important feature of the CANDLE design is that the natural chromaticity of the machine  $\xi_x = -18.9$  in horizontal and  $\xi_y = -14.8$  in vertical planes is compensated by two families of focusing (SF) and defocusing (SD) sextupoles located at the double bend section (Figure 3.1.6). For the given sextupole magnets length, 21 mm for SF and 25 mm for SD, the strengths of the sextupoles that compensate the linear chromaticity of the storage ring are  $29.7 \text{ m}^{-3}$  and  $35.1 \text{ m}^{-3}$  respectively. The sextupole magnets compensating the linear chromaticity of the machine induce, in turn, nonlinear motion into the electron trajectories which results in amplitude-dependent tune variations and, ultimately, unstable motion at an oscillation amplitude which defines the dynamic aperture.

Figure 3.1.7 shows the radial (top) and vertical (bottom) phase-space trajectories of on and off-energy ( $\Delta E/E = \pm 3\%$ ) electrons in the middle of the straight section tracked over 1000 turns in the ring with the initial amplitudes of 15 mm when the chromaticity is compensated to zero. The distortion of the trajectories from their linear elliptical shape, caused by the sextupole fields, is apparent.



**Fig. 3.1.7 Trajectories of on and off-energy ( $\Delta E/E = \pm 3\%$ ) electrons in the middle of the straight section tracked over 1000 turns in the ring with the initial amplitudes of 15mm.**

The dynamic aperture, i.e. the local projection of the phase space acceptance to physical space, in the middle of the straight section is shown in Fig. 3.1.8. These values have been used to specify the beam-stay –clear region and, in turn, the magnet apertures.



**Fig. 3.1.8 Dynamic aperture of the storage ring in the center of straight section.**

In analyzing the expected performance of the storage ring, there are two other parameters that define the stable and flexible operation of the machine: the amplitude dependent betatron tune shift and the momentum-dependent tune shift.

To avoid resonance crossings, the amplitude-dependent tune shift must remain within reasonable values. Fig. 3.1.9 presents the amplitude-dependent tune shift as a function of the emittance. Betatron amplitude values were taken as the square of the magnitude of fundamental peak of betatron trajectory Fourier spectrum divided by the local beta function. Close to the stability limit, the dynamics becomes nonlinear, and the amplitudes of high harmonics increase at the expense of the fundamental betatron frequency thereby causing the curve to bend back. In the case of CANDLE, the tunes do not approach half integer until the betatron amplitude  $a_\beta$  in the horizontal and vertical planes exceeds 20 mm, which corresponds to the emittance of about  $\varepsilon = 40 \mu m$ .

Since individual particles within the electron beam undergo energy oscillations, it is important also to minimize the energy-dependent tune shift caused by the beta function distortion of the off-energy particles. Fig. 3.1.10 shows the resulting peak  $\beta$  function distortion as a function of energy. The corresponding plot of energy-dependent tune shifts in the horizontal and vertical planes is shown in Fig. 3.1.11. Due to the low chromatic variation of the  $\beta$ -functions, the rise of the off-energy dynamic aperture is observed for energy spreads that exceed 3%. Note, that the rms energy spread of the particles in CANDLE storage ring is at the level of 0.1%.

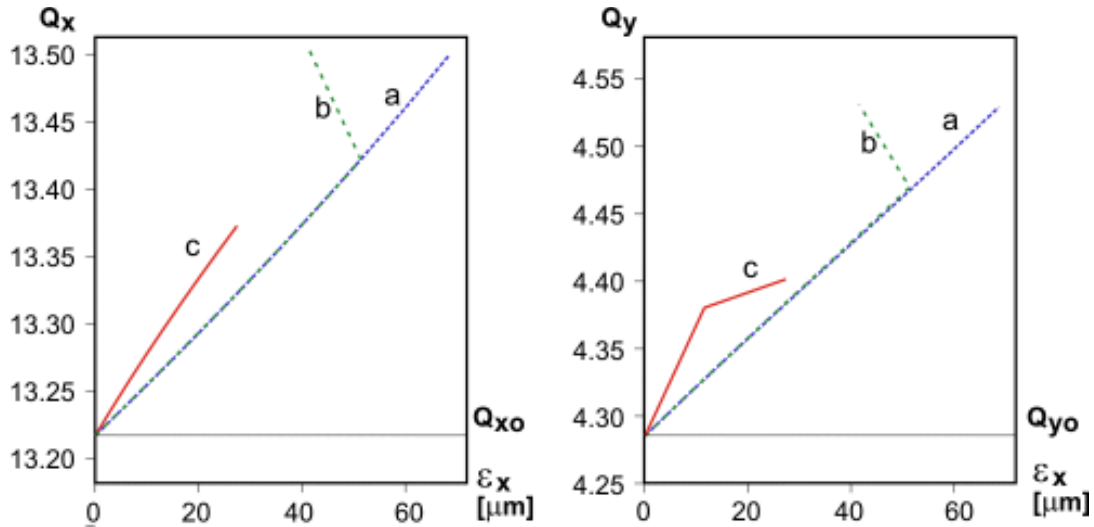


**Fig. 3.1.9** The amplitude-dependent horizontal (left) and vertical (right) tune shifts after particle tracking over 512 turns. a) zero coupling, b) 1% coupling, c) 100% coupling.

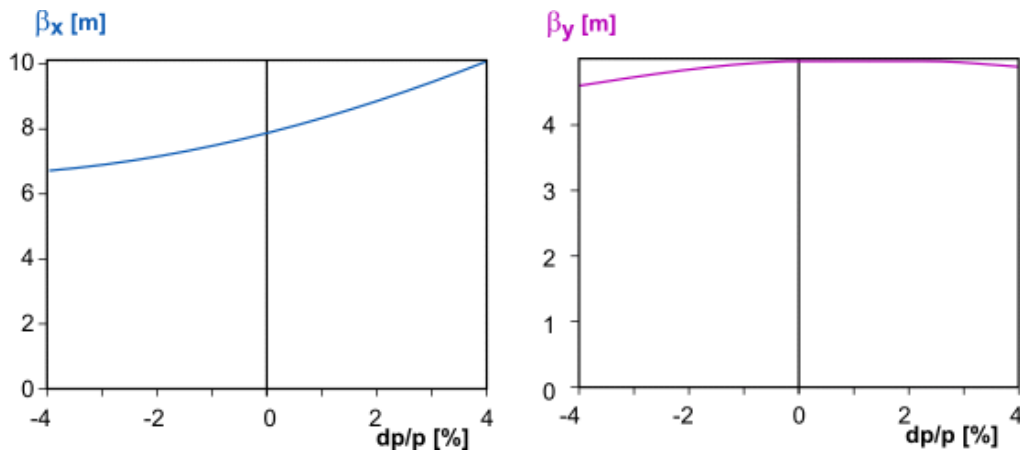


**Fig. 3.1.10** Momentum dependent horizontal (left) and vertical (right) beta functions at the symmetry point of straight section.

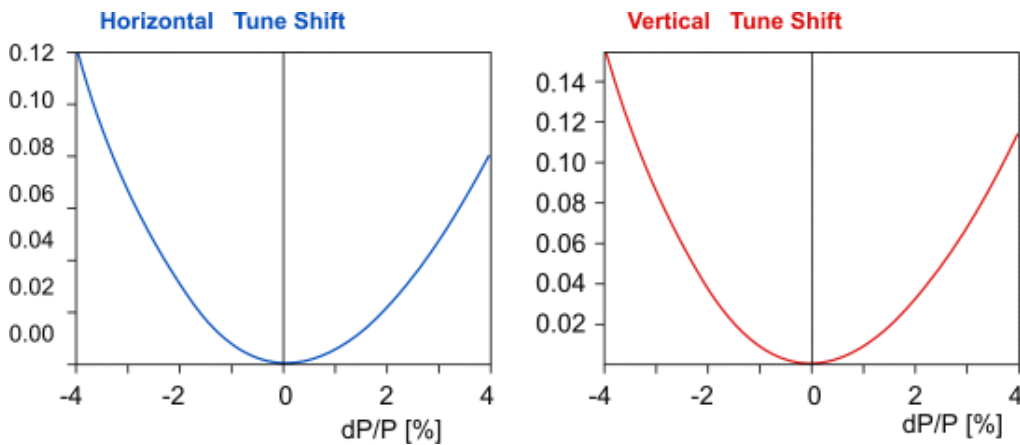


**Fig. 3.1.11** The horizontal (left) and vertical (right) tune shifts as a function of particle energy.

The results of tracking simulation provide the momentum acceptance limitations caused by the beam pipe aperture and are shown in Fig.3.1.12 for horizontal (top) and vertical (bottom) transverse modes respectively. The beam pipe defines the geometric acceptances (line **a**) simply given by  $A = R^2 / \beta_{\max}$  with  $R$  -beam pipe radius and  $\beta_{\max}$  -maximum beta function. The dynamical aperture bound dependence on the energy deviation is shown by curve **b**. The central dotted line **c** indicates the closed orbit deviation due to chromatic errors. Note, that for the particles with negative horizontal displacement, the geometrical and dynamic apertures actually coincide.

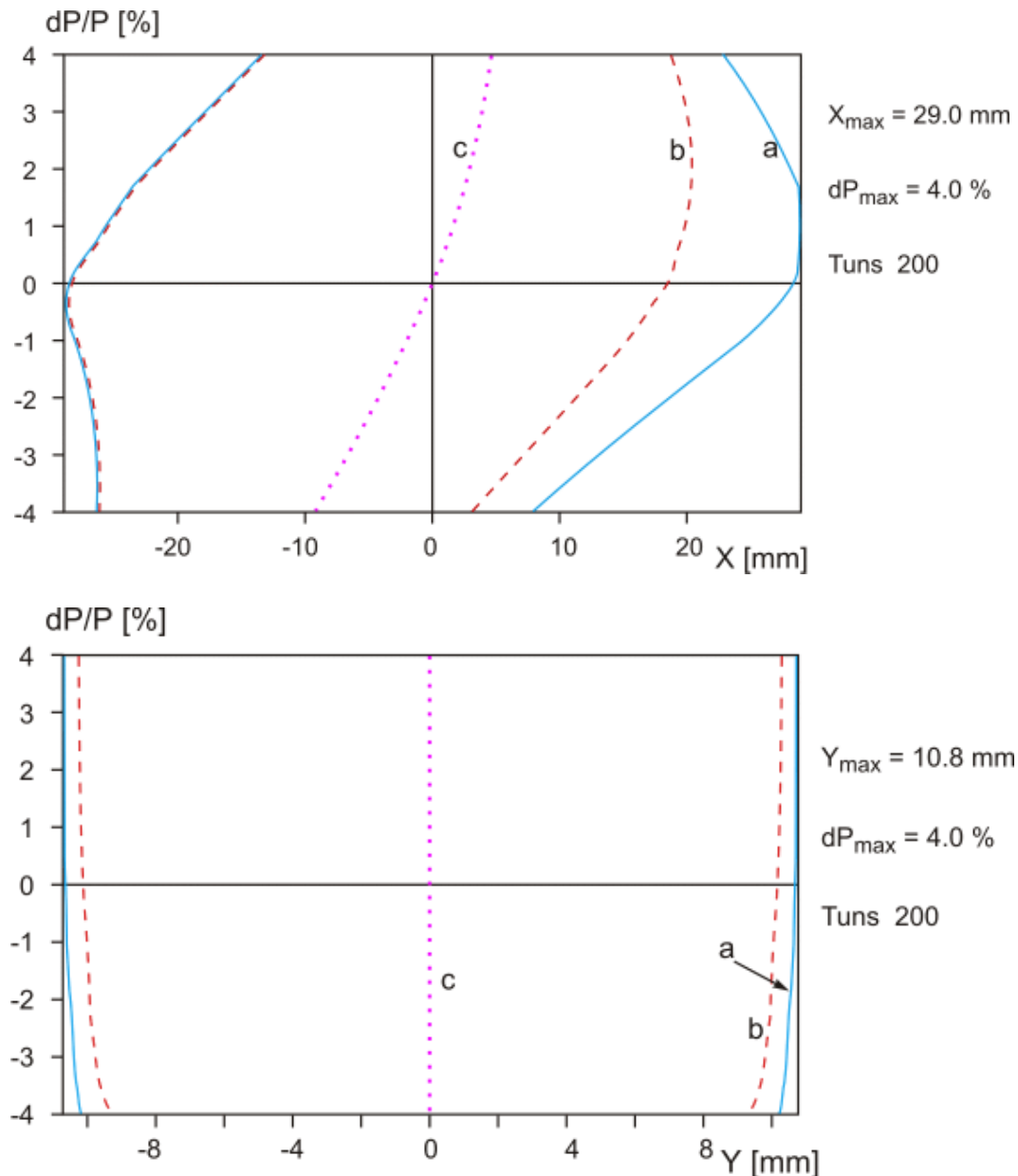


**Fig. 3.1.12 Momentum acceptances given by the horizontal and vertical apertures as a function of relative momentum deviation in the center of straight section. Shown are the horizontal (top) and vertical (bottom) dynamic (curves a) and geometric apertures (curve b). The central line is momentum dependent closed orbit (c).**

Fig. 3.1.13 (left) shows the dependence of the beam natural emittance on the synchronous particle energy deviation taking into account the chromatic change of the lattice functions. A 10% emittance growth is observed for a positive energy deviation of 1.5%. The absolute energy of the beam in the CANDLE storage ring will be kept constant at a level better than 0.1%, so the emittance will be stabilized in the lattice to an accuracy of better than 0.5%. Fig. 3.1.13 (right) shows a very smooth dependence of beam energy spread on the synchronous particle energy deviation at 3 GeV. For the relative energy deviation of 1% the change in energy spread is below 0.5%.

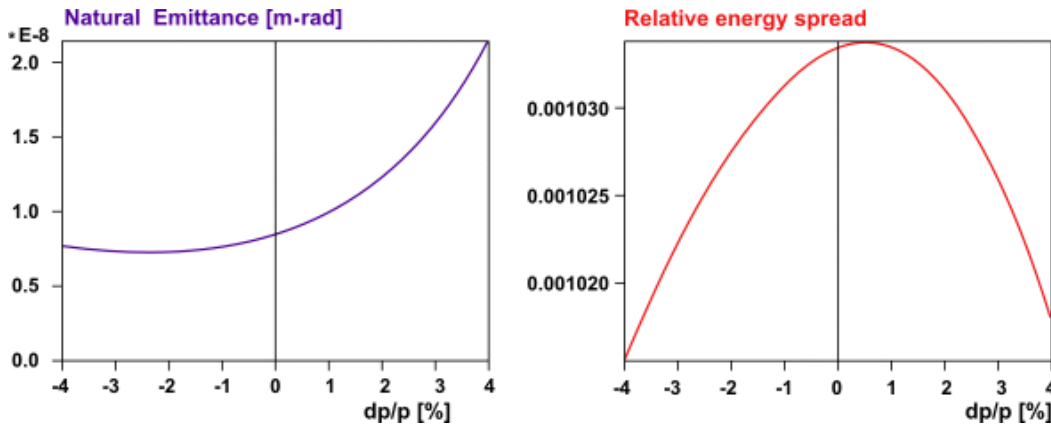


**Fig. 3.13 Natural emittance (left) and relative energy spread (right) dependence on the synchronous particle energy deviation at 3 GeV.**

### 3.1.5 Magnet Parameters

The storage ring contains 32 bend magnets, 80 quadrupoles, and 64 sextupoles. The magnets lengths, fields and locations are chosen so that to minimize emittance and the beta function, to allow ample space in the straight sections, as well as to maximize the dynamic aperture and operational stability. Table 3.1.4 presents the main geometrical parameters of the magnets and the required magnetic fields.

The lattice design provides 16 symmetric cells along the storage ring. In order to increase the magnet system lifetime and the reliability, as well as to provide some flexibility in the operating parameter space, the maximum strength of the magnets will be 15- 20% greater than the nominal required strength for 3 GeV electrons. Based on the dynamical aperture study for the ring, the dipole magnet gap has been optimized to 44 mm, while the apertures of the quadrupoles and sextupoles are 35 and 40 mm respectively. The apertures of the magnets and design features are adjusted with the vacuum chamber geometry and the assembling requirements. The mechanical and electrical considerations of the magnets are given in the separate section.

The nominal magnets parameters, given for 3 GeV electrons energy, provide 8.4 nm-rad horizontal emittance for the electron beam. To achieve this emittance with 16 periods, in addition to electron bend the dipole magnets have the magnetic gradient of 3.3 T/m that provides an additional vertical focusing of the electrons. All the magnets are the room temperature conventional ones based on the well-proven technology.

**Table 3.1.4 Storage ring magnet parameters for 3 GeV.**

<b>Magnet type</b>	<b>Nominal value at 3 GeV</b>	<b>Magnet Limit</b>
<b>Dipoles</b> Quantity	<b>32</b>	
Dipole gap height (mm)	44	
Effective length (m)	1.45	
Dipole field B (T)	1.345	1.7
Dipole gradient $G_B$ (T/m)	-3.3	3.3
<b>Quadrupoles</b> Quantity	<b>80</b>	
Aperture radius (mm)	35	
<b>QF</b> Strength ( $m^{-2}$ )	<b>1.649</b>	
Gradient (T/m)	16.5	20
Pole tip field (T)	0.58	0.7
Effective length	0.38	
<b>QD</b> Strength ( $m^{-2}$ )	<b>1.289</b>	
Gradient (T/m)	12.9	20
Pole tip field (T)	0.45	0.7
Effective length (m)	0.16	
<b>QFC</b> Strength ( $m^{-2}$ )	<b>1.703</b>	
Gradient (T/m)	17.04	20
Pole tip field (T)	0.595	0.7
Effective length (m)	0.5	
<b>Sextupoles</b> Quantity	<b>64</b>	
Aperture radius (mm)	40	
<b>SF</b> Strength ( $m^{-3}$ )	<b>29.7</b>	
$B''$ ( $T/m^2$ )	297	440
Pole tip field (T)	0.237	0.35
Effective length (m)	0.21	
<b>SD</b> Strength ( $m^{-3}$ )	<b>35.1</b>	
$B''$ ( $T/m^2$ )	351	440
Pole tip field (T)	0.28	0.35
Effective length (m)	0.25	

## Reference

1. M. Sands, “ Introduction to Storage Ring”, SLAC –191, 1971.
2. P. Bellomo et al, SPEAR3 Design Report, SSRL, August, 1999.
3. H. Wiedemann, “Particle Accelerator Physics I”, Springer-Verlag, Berlin, 1999.
4. J. Corbett, T. Rabedeau, Synchrotron Radiation News 12, 22, 1999.
5. V. Tsakanov et al, Rev. Sci. Instrum. **73**:1411-1413, 2002.
6. H. Wiedemann, “Electromagnetic Radiation from Relativistic Electron Beams”, SSR, Nov. 13-16, ICTP, Trieste, Italy, 2000.
7. M. Ivanian, Y. Martirosyan, V. Tsakanov, EPAC 2002
8. Y.L. Martirosyan, M.I. Ivanian, V.M. Tsakanov, Proc. of “*Electron-Photon Interaction in Dense Media*”, Nor-Amberd, June 2001, Kluwer Academic Publishers, edited by H. Wiedemann, v. **49**, pp. 349-357, 2002
9. C. Pellegrini, Nuovo Cimento A **64**, 447, 1969.
10. M. Sands, SLAC Reports TN-69-8 and TN 69-10, 1969.